Degree Project in Applied Physics

Second cycle, 30 credits

Towards understanding magnetization in underwater naval systems

Measuring magnetic properties in steel subject to water pressure induced stress

NIKLAS KÄLL

Towards understanding magnetization in underwater naval systems

Measuring magnetic properties in steel subject to water pressure induced stress

NIKLAS KÄLL

Master's Programme, Engineering Physics, 120 credits
Date: June 22, 2026

Supervisors: Viktor Djurberg, Nanna Zhou Hagström, Henrik Åkerstedt
Examiner: Magnus Andersson
School of Engineering Sciences
Host company: Swedish Defence Research Agency (FOI)
Swedish title: Mot en ökad förståelse av magnetisering i undervattensfarkoster
Swedish subtitle: Mätning av magnetiska egenskaper hos stål utsatt för vattentrycksinducerad spänning

© 2026 Niklas Käll

Abstract

Stealth is a key attribute of underwater naval systems, many of which are built from ferromagnetic materials such as steel. These materials can retain a permanent magnetization, producing a detectable magnetic signature, so vessels are typically demagnetized before deployment. When submerged, however, water pressure imposes compressive stress on the hull, which can reintroduce magnetization via the Villari effect. This thesis investigates the relationship between compressive stress and the magnetic properties of ferromagnetic materials under high water pressure conditions.

An experimental setup was constructed to measure the magnetization of a steel core sample under controlled compressive stress, using a hydraulic press and a two-solenoid arrangement to generate an applied field and measure magnetic flux. Two experiments were performed. In the first, hysteresis loops were recorded under an alternating applied field at several constant stress levels. The loops widened with increasing stress, corresponding to increased magnetic coercivity and decreased remanence. In the second experiment, the change in magnetization was measured under a constant applied field while the stress was varied. A fully magnetized sample showed a clear decrease in magnetization with stress at all but the strongest applied field, whereas the demagnetized sample exhibited more complex behavior.

The observed stress dependence is consistent with magnetoelastic theory for a material with positive saturation magnetostriction, in which compressive stress drives domains away from the stress axis. Eddy currents were found to influence the alternating-field measurements significantly, even below 1 Hz, limiting those results to a qualitative interpretation. The findings indicate that the stress dependence of magnetic properties should be accounted for when counteracting the magnetic signature of underwater naval systems.

Keywords

Magnetism, Ferromagnetism, Villari effect, Magnetoelastic coupling, Magnetic hysteresis, Coercivity, Remanence, Demagnetization, Underwater naval systems

Sammanfattning

Smygförmåga är en central egenskap hos undervattensfarkoster, varav många är byggda av ferromagnetiska material såsom stål. Dessa material kan behålla en permanent magnetisering och därmed ge upphov till en detekterbar magnetisk signatur, varför farkoster vanligtvis avmagnetiseras innan användning. Vid nedsänkning utsätter dock vattentrycket skrovet för tryckspänning, vilket kan återintroducera magnetisering via Villari-effekten. Detta examensarbete undersöker sambandet mellan tryckspänning och de magnetiska egenskaperna hos ferromagnetiska material under förhållanden med högt vattentryck.

En experimentuppställning konstruerades för att mäta magnetiseringen hos ett stålprov i form av en kärna under kontrollerad tryckspänning, detta med hjälp av en hydraulisk press och en uppställning bestående av två solenoider för att generera ett pålagt fält och mäta det magnetiska flödet. Två experiment genomfördes. I det första undersöktes hystereskurvor under ett alternerande pålagt fält vid flera konstanta spänningsnivåer. Kurvorna vidgades med ökande spänning, vilket motsvarar ökad koercivitet och minskad remanens. I det andra mättes förändringen i magnetisering under ett konstant pålagt fält medan spänningen varierades. Ett fullt magnetiserat prov uppvisade en tydlig minskning av magnetiseringen med spänning vid alla fält utom det starkaste, medan det avmagnetiserade provet uppvisade ett mer komplicerat beteende.

Det observerade spänningsberoendet stämmer överens med magneto-elastisk teori för ett material med positiv magnetostriktionskonstant, där tryckspänning driver domänerna bort från spänningsaxeln. Virvelströmmar visade sig påverka mätningarna i alternerande fält avsevärt, även vid frekvenser lägre än 1 Hz, vilket begränsar dessa resultat till en kvalitativ tolkning. Resultaten indikerar att magnetiska egenskapers spänningsberoende bör beaktas vid utformningen av motmedel mot undervattensfarkosters magnetiska signatur.

Nyckelord

Magnetism, Ferromagnetism, Villari-effekten, Magnetoelastisk koppling, Magnetisk hysteres, Koercivitet, Remanens, Avmagnetisering, Undervattens-farkoster

Acknowledgments

I wish to sincerely thank my supervisors at FOI, Viktor Djurberg, Nanna Zhou Hagström, and Henrik Åkerstedt, not only for their amazing guidance throughout this project, but also for making my time at FOI a genuinely fun experience. I extend my gratitude to all my coworkers at FOI, who have continuously shown interest and support towards my thesis.

Furthermore, I wish to thank my examiner, Magnus Andersson, for making this thesis possible and for providing excellent feedback.

Finally, I want to thank my friends and family for their endless support and encouragement throughout my education.

Stockholm, June 2026
Niklas Käll

Contents

1 Introduction **1**
1.1 Purpose . . . 1
1.2 Goals . . . 2
1.3 Scope and delimitations . . . 2
1.4 Structure of the thesis . . . 2

2 Background and methods **3**
2.1 Fundamentals of ferromagnetism . . . 3
2.1.1 Hysteresis . . . 4
2.1.2 Demagnetization using alternating current . . . 5
2.2 Magnetostriction and the Villari Effect . . . 6
2.3 Measuring magnetization . . . 7
2.3.1 Loss of magnetic flux due to gap . . . 8
2.3.2 Heat generation . . . 9
2.4 Eddy Currents . . . 9
2.4.1 Diffusion equation in the quasi-static limit . . . 10
2.4.2 Joule dissipation . . . 10
2.5 Power loss . . . 11
2.6 Stress on underwater vessels . . . 11

3 Experimental setup **14**
3.1 Samples . . . 14
3.1.1 Stress distribution . . . 15
3.1.2 Copper solenoids . . . 16
3.2 Circuit . . . 18
3.3 Signal generation and data collection . . . 18
3.3.1 Sample rate . . . 19
3.4 Output signal . . . 19
3.5 Data processing . . . 20

3.5.1 Field calculations 20
3.5.2 Noise correction 21
3.6 Effect of eddy currents 22

4 Experiment 1 **25**
4.1 Objective 25
4.2 Experiment procedure 25
4.3 Results and analysis 26

5 Experiment 2 **28**
5.1 Objective 28
5.2 Experiment procedure 28
5.3 Results and analysis 29

6 Discussion **33**
6.1 Limitations 34
6.2 Conclusions 34
6.3 Future work 35
6.3.1 Possible setup improvements 35
6.3.2 Further experiments 35
6.4 Use of AI tools 36

References **37**

List of Figures

2.1 Magnetic domain structure of NdFeB, image by Gorchy, Wikimedia Commons, CC BY-SA 3.0 [3]. 4
2.2 Typical shape of a $H-M$ hysteresis loop. Magnetic coercivity and remanence are marked as H_c and M_r, respectively. 5
2.3 Theoretical circuit diagram of the experiment, capable of measuring magnetization. A ferromagnetic sample in the middle in the shape of a rectangular core. 7
2.4 Hull subject to water pressure. 12
2.5 Simulation of hull displacement and internal stresses at 3.30MPa water pressure. 12

3.1 Sample blueprint, measurements in mm. 15
3.2 FEM simulation of the steel sample under 250 kN load. 16
3.3 Circuit diagram of the experimental setup. 18
3.4 H-M diagram plotted in Python using measured voltage data. . 21
3.5 Noise signal and noise integral over a 0.5 second interval. . . . 22
3.6 H-M loops measured at various frequencies with extrapolated loop $f \to 0$ in black. 23
3.7 Comparison between predicted H-M loop using Bertotti model and measured H-M loop for $f = 0.25$Hz. 24

4.1 Average magnetization measured in the direction of stress against applied field strength, measured at six different loads using 15A, 0.025Hz, Direct Current (DC)-offset corrected and applied Savitzky–Golay filter with window size of 501. 26
4.2 Mean magnetic coercivity and remanence of the sample measured in the direction of stress against compressive stress, calculated from three loops, measured using 15A, 0.025Hz. Error bars show standard deviation across the three measurements. 27

5.1 Change in magnetization measured in the direction of stress against applied stress in a fully magnetized sample subject to various constant applied field strengths. 29
5.2 Change in magnetization measured in the direction of stress against applied stress in a demagnetized sample subject to various constant applied field strengths. 31

List of Tables

3.1 Properties of the sample. 15

5.1 Current of DC signals used and corresponding field strengths in the solenoid. 29

List of acronyms and abbreviations

AC	Alternating Current
cRIO	compact real-time embedded industrial controller
DC	Direct Current
FEM	Finite Element Method
FPGA	Field Programmable Gate Array
IO	input/output
LUT	Lookup Table

Chapter 1

Introduction

Stealth is a key attribute in many underwater naval systems. Consequently, many detection technologies have been developed to locate such systems. These detection strategies are categorized into acoustic and non-acoustic systems. Acoustic systems rely on sound detection, using either active or passive sonar. Non-acoustic systems exploit other physical traces, including trace chemicals, thermal changes, and radioactivity. One of these technologies is based on measuring the magnetic fields of underwater vessels.

Specifically, these technologies exploit the fact that underwater naval systems are primarily constructed from ferromagnetic materials such as steel, which can carry permanent magnetization, thereby producing a magnetic field. This then allows detections by identifying small disturbances in Earth's magnetic field. To combat this, vessels often undergo a process called demagnetization before deployment. This process aims to eliminate the magnetic field, however, as the vessel is submerged deep below the surface, the water pressure introduces a new problem. The pressure creates stress in the exterior of the vessel. This stress then has the potential to reintroduce magnetization in the ferromagnetic material due to a phenomenon known as the Villari effect. It is crucial to understand this phenomenon when constructing underwater systems and their detection counterparts.

1.1 Purpose

The purpose of this thesis is to strengthen the knowledge about the correlation between magnetic properties and stress in ferromagnetic materials in the context of high water pressure conditions, and to better understand this problem in regard to underwater naval systems.

1.2 Goals

1. Construct an experimental setup with the ability to measure the magnetization of samples subjected to compressive stress.
2. Conduct measurements using said setup and find key magnetic properties for steel under forces of different amplitudes.
3. To draw conclusions and make generalizations from these values in the context of underwater naval systems.

1.3 Scope and delimitations

To fully understand the magnetization of underwater vessels is not a simple task. It requires a vast amount of information about the geometry of the system and the forces involved. Although the complete picture of magnetization in these systems is beyond the scope of this thesis, by breaking down the system into its components and applying forces of realistic amplitudes, the aim is to draw conclusions on a bigger scale.

1.4 Structure of the thesis

Chapter 2 presents relevant background theory regarding ferromagnetism and water pressure. It also discusses methods used on a conceptual level and presents the necessary equations later used. Chapter 3 provides a detailed description of the experimental setup, including information about the construction process. The two experiments that were conducted using this setup are explained in chapters 4 and 5. Here, the objectives, procedures, and results of each experiment are presented in their respective chapter. Finally, 6 covers conclusions and reflections of the project as a whole.

Chapter 2

Background and methods

This chapter presents the theory necessary to understand the concepts underlying the experimental setup. It begins with the fundamentals of ferromagnetism, including magnetic domains and hysteresis, before introducing magnetostriction and the Villari effect, which form the basis for the stress dependence studied in this work. The principle behind measuring magnetization is then described, along with practical considerations, as well as the role of eddy currents and the associated power losses. Finally, a brief overview of the stress conditions experienced by submerged vessel hulls.

2.1 Fundamentals of ferromagnetism

Ferromagnetic materials exhibit the property of considerably high magnetic permeability, which is to say that they gain a significant magnetization in response to an applied field. Many of these materials also exhibit high magnetic coercivity, enabling them to withstand stronger external fields without becoming demagnetized. Lastly, they often exhibit high magnetic remanence, meaning they remain magnetized after the external field is removed. These properties allow ferromagnets to become permanent magnets.

The origin of these properties is found at the atomic scale. Each atom in a ferromagnetic material carries a magnetic moment, arising primarily from the spin of its electrons. In most materials, these moments are randomly oriented and average out, but in ferromagnets, a quantum mechanical exchange interaction favors the parallel alignment of neighboring moments, giving rise to a spontaneous magnetization even in the absence of an applied field [1].

When atomic magnetic dipoles align themselves with their neighbors, they do this in groups called domains. Each domain contains billions of dipoles

oriented in the same direction, however, domains are not necessarily oriented parallel to each other. In a demagnetized ferromagnetic material, the domains are randomly oriented, causing their magnetic fields to cancel out. The more domains that are aligned, the stronger the magnet becomes [2].

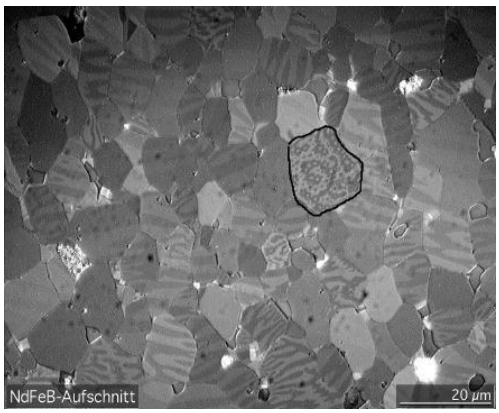

Figure 2.1: Magnetic domain structure of NdFeB, image by Gorchy, Wikimedia Commons, CC BY-SA 3.0 [3].

2.1.1 Hysteresis

This permanent magnetization is caused by a phenomenon called hysteresis. When an external field is applied to a ferromagnet, the magnetic domains in that material will align with that field to some degree. When the external field is removed, the alignment partially persists, and the material is magnetized. Furthermore, the relationship between the magnetization of the material and its magnetic field follows a characteristic curve referred to as a hysteresis loop.

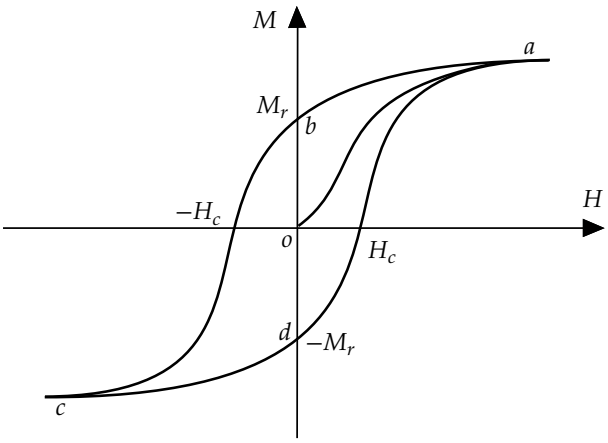

Figure 2.2: Typical shape of a $H - M$ hysteresis loop. Magnetic coercivity and remanence are marked as H_c and M_r, respectively.

Suppose that the material initially has no magnetization and that the applied field starts at zero ($M = H = 0$). As the applied field increases, the magnetization curve follows the initial magnetization curve *oa*, where magnetization increases rapidly until it reaches magnetic saturation. At this point, all domains are aligned, and the material is at its maximum magnetization. As the applied field is then decreased, it now follows the *abc* curve. As can be seen, the relationship no longer passes the origin, instead at $H = 0$, there is a remanent magnetization M_r. It is not until the applied field reaches $-H_c$ that the magnetization is zero. Here, H_c is the magnetic coercivity. If the curve then reaches negative magnetic saturation, and the applied field is again increased, the relationship now follows the *cda* curve, completing the *abcda* hysteresis loop [4].

2.1.2 Demagnetization using alternating current

There are multiple ways of demagnetizing a ferromagnet, but the common principle is to perform an action that disrupts the alignment of domains. To achieve a near perfect demagnetization, the main goal is to have the domains randomly oriented across the whole sample. One method is to expose the sample to a series of external fields with alternating opposite directions that slowly weaken over time, achieved by sending a decaying Alternating Current (AC) signal through a solenoid containing the sample.

As the alternating current is applied, the magnetization will follow a hysteresis curve such as the one in Fig. 2.2, where each period of the current

will correspond to one loop in the diagram. As the current, and thereby the applied field, slowly decreases, the loop will ”shrink”, bringing the points b and d closer to zero. Then, when the current's amplitude is sufficiently close to zero, and is then turned off, the remanent magnetization will be close to none, leaving the sample demagnetized [4].

2.2 Magnetostriction and the Villari Effect

Magnetostriction describes the relationship between the magnetic state and mechanical strain of a ferromagnetic material. When a ferromagnet is magnetized, it undergoes a small dimensional change along the magnetization axis. The magnitude and sign of this effect is characterized by the saturation magnetostriction constant λ_s, where a positive value indicates elongation along the magnetization direction and a negative value indicates contraction [1]. The sign of λ_s is material-dependent and fundamentally governs how a ferromagnet responds to mechanical stress.

The energy associated with the interaction between mechanical stress and the magnetic domain structure is captured by the magnetoelastic energy, given by

$$E_{\text{me}} = \frac{3}{2}\lambda_s \sigma \sin^2 \theta \tag{2.1}$$

where σ is the applied stress and θ is the angle between the magnetization direction and the stress axis [1]. This expression shows that the energetic preference of a domain depends directly on the sign of the product $\lambda_s\sigma$. For a material with $\lambda_s > 0$, tensile stress ($\sigma > 0$) lowers the energy of domains aligned parallel to the stress axis ($\theta = 0$), making that orientation energetically favorable. Conversely, compressive stress ($\sigma < 0$) makes the parallel orientation unfavorable, driving domains toward configurations perpendicular to the stress axis. For a material with $\lambda_s < 0$, the opposite is true.

The Villari effect, sometimes referred to as the inverse magnetostriction, is the direct consequence of this energy configuration [5]. When mechanical stress is applied to a demagnetized sample, domains are free to reorient toward whichever configuration minimizes the total energy. For a material with $\lambda_s > 0$ under tensile stress, this results in a spontaneous increase in magnetization along the stress axis. Under compressive stress, domains are instead driven into the plane perpendicular to the stress axis.

The sign of λ_s is not necessarily constant, but can vary based on the applied

field strength. Iron has $\lambda_s > 0$ only when the applied field strength is less than approximately $\pm 40 \text{kA/m}^2$, while nickel always has $\lambda_s < 0$ [1].

2.3 Measuring magnetization

The circuit in Fig. 2.3, inspired by Baynes's setup [6], is an example of how magnetization can be measured given a sample shaped like a closed magnetic core, and it relies on detecting changes in magnetic flux. The theoretical setup is divided into two parts. Circuit 1 controls a current which is driven through the left solenoid (solenoid 1) on the sample, generating an applied field H_z in the z-direction. If any change in flux occurs in the sample, caused by either a varying current in solenoid 1 or by an alternation in the sample's magnetization, it will induce a voltage across circuit 2, with the help of the right solenoid (solenoid 2).

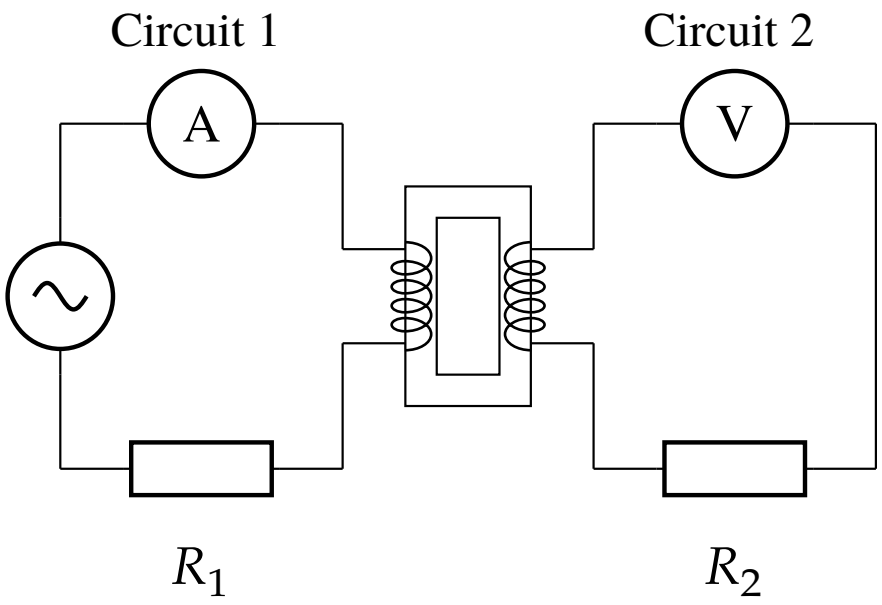

Figure 2.3: Theoretical circuit diagram of the experiment, capable of measuring magnetization. A ferromagnetic sample in the middle in the shape of a rectangular core.

The magnetic flux density $\boldsymbol{B}$, the applied field $\boldsymbol{H}$ and magnetization $\boldsymbol{M}$

follows relationship

$$\boldsymbol{B} = \mu(\boldsymbol{H} + \boldsymbol{M}) \quad \Longrightarrow \quad \boldsymbol{M} = \frac{\boldsymbol{B}}{\mu} - \boldsymbol{H}. \tag{2.2}$$

In regard to the setup in Fig. 2.3, define B_z as the magnetic flux density in the solenoid of circuit 2. B_z can be found by measuring the voltage V_2 across circuit 2 and applying the relation

$$V_2 = -N_2 A_{\text{core}} \frac{dB_z}{dt} \quad \Longrightarrow \quad B_z = -\frac{1}{N_2 A_{\text{core}}} \int V_2 \, dt \tag{2.3}$$

where A_{core} is the cross-sectional area of the sample's side segments and N_2 is the number of loops in solenoid 2. The next step is to find the contribution of the applied field $\boldsymbol{H}$ to B_z, which can be done by measuring the current I_1 in circuit 1 and using the approximation

$$\oint \boldsymbol{H} \cdot d\boldsymbol{\ell} \approx H_z \, \ell_m = I_1 \, N_1 \quad \Longrightarrow \quad H_z = \frac{N_1}{\ell_m} I_1 \tag{2.4}$$

where ℓ_m is the mean magnetic path length of the sample and N_1 is the number of loops in solenoid 1. Lastly, the magnetization can be calculated by subtracting the contribution of the applied field from the field measured in solenoid 2.

$$M(t) = -\frac{1}{N_2 A_{\text{core}} \mu_0} \int V_2(t) \, dt \; - \; \frac{N_1}{\ell_m} I_1(t) \tag{2.5}$$

Furthermore, given a data set I_1 and V_2 values, these equations can be used to plot a hysteresis diagram of the sample.

2.3.1 Loss of magnetic flux due to gap

In the setup above, if there is a gap between the solenoid and the magnetic core, the magnetic flux inside the core is affected by the presence of air in the solenoid. The total magnetic flux produced by the solenoid is distributed across the cross-sectional area A_{tot} inside the solenoid, while the core occupies only $A_{\text{core}} < A_{\text{tot}}$. Since magnetic flux is solenoidal ($\nabla \cdot \mathbf{B} = 0$), it is conserved across any cross-section, and the flux density in the core and in the surrounding air gap are related by the boundary condition on the normal component of $\mathbf{B}$ [2].

In the limit of high core permeability ($\mu_r \gg 1$), the reluctance of the core

is negligible compared to that of the air gap, and the field inside the solenoid is approximately uniform across A_{tot}. The flux threading the core is then simply a geometric fraction of the total flux,

$$\frac{\Phi_{\text{ag}}}{\Phi_0} = \frac{A_{\text{core}}}{A_{\text{tot}}}, \tag{2.6}$$

where Φ_{ag} and Φ_0 are the magnetic flux through the core with and without the gap, respectively.

2.3.2 Heat generation

Any current traveling in a material with non-zero resistance will generate heat in a process called Joule heating. This is a relevant consideration for the solenoids in the setup, as heat can change the wire's resistance and potentially damage its insulating coating. Using AC, the average power, P_{avg}, generated is given by

$$P_{avg} = RI_{rms}^2 = \rho\frac{L}{A}I_{rms}^2 \tag{2.7}$$

where I_{rms} is the root-mean-square current and $R = \rho\frac{L}{A}$ is the resistance, with ρ, L, A being the resistivity, length, and cross-sectional area of the wire [2].

2.4 Eddy Currents

Given an electrically conductive magnetic core, an applied magnetic field that varies in time will induce currents within the core according to Maxwell's equations.

$$\nabla \times \boldsymbol{E} = -\frac{\partial \boldsymbol{B}}{\partial t}. \tag{2.8}$$

The induced electric field in turn drives a current density in the conductor through Ohm's law,

$$\boldsymbol{j} = \sigma \boldsymbol{E}, \tag{2.9}$$

where $\boldsymbol{j}$ is the current density and σ the electrical conductivity. The circulating currents produced in this way are known as eddy currents, and they dissipate the field energy into heat through resistance [7].

2.4.1 Diffusion equation in the quasi-static limit

In good conductors and at moderate frequencies, the conduction current density greatly exceeds the displacement current, $\sigma \gg \varepsilon_0 \varepsilon_r \omega$, so the displacement term in Ampère's law may be neglected [7]. In this quasi-static regime,

$$\nabla \times \boldsymbol{H} = \boldsymbol{j}. \tag{2.10}$$

Combining Eq. (2.10) with Ohm's law, Faraday's law, and the constitutive relation $\boldsymbol{B} = \mu_0 \mu_r \boldsymbol{H}$ for a homogeneous medium, and using $\nabla \cdot \boldsymbol{B} = 0$, one obtains a diffusion equation for the magnetic field inside the core,

$$\nabla^2 \boldsymbol{H} = \mu_0 \mu_r \sigma \frac{\partial \boldsymbol{H}}{\partial t}. \tag{2.11}$$

The same equation is satisfied by $\boldsymbol{E}$ and $\boldsymbol{j}$. For a harmonic excitation varying as $\exp(-i\omega t)$, this reduces to the Helmholtz form

$$\nabla^2 \boldsymbol{H} = -i\, \mu_0 \mu_r \sigma \omega\, \boldsymbol{H}, \tag{2.12}$$

from which a characteristic length scale, the magnetic skin depth, can be defined as

$$\delta = \sqrt{\frac{2}{\mu_0 \mu_r \sigma \omega}}. \tag{2.13}$$

The magnetic field, the induced electric field, and the eddy currents all decay into the conductor on this scale. In ferromagnetic core materials $\mu_r \gg 1$, so δ can be very small even at lower frequencies.

2.4.2 Joule dissipation

Because $\boldsymbol{j} \cdot \boldsymbol{E} = \sigma E^2 \geq 0$, the work done by the field on the eddy currents is irreversibly converted into heat. The time-averaged power loss in a volume V is

$$P_{\text{loss}} = \int_V \boldsymbol{j} \cdot \boldsymbol{E}\, dV = \int_V \sigma E^2\, dV. \tag{2.14}$$

In the low-frequency regime, where $E \propto fB$, this implies that the volumetric loss density scales as $f^2 B^2$.

2.5 Power loss

When driving a magnetic core with an AC field, Bertotti's model can be used to calculate the total energy loss. The power loss model consists of three components in which energy is converted into heat. The first component is caused by the hysteresis itself. Each cycle, as domain walls rotate, a fixed amount of energy is wasted. As such, this effect scales linearly with frequency, $P_{\text{hys}} \propto f$. The second component comes from the previously discussed classical eddy currents. As stated, this component scales as $P_{\text{eddy}} \propto f^2$. The last component also arises from eddy currents, but this time locally from each individual domain rotation. Around each domain wall, there is a localized eddy-current loop, and as Bertotti shows, their dissipation loss scales as $P_{\text{exc}} \propto f^{\frac{3}{2}}$ [8]. Putting these the resulting power loss is given by

$$P_{\text{tot}} = P_{\text{hys}} + P_{\text{eddy}} + P_{\text{exc}} \tag{2.15}$$

$$P_{\text{tot}}(B,f) = k_{\text{hys}}(B)f + k_{\text{eddy}}(B)f^2 + k_{\text{exc}}(B)f^{\frac{3}{2}} \tag{2.16}$$

Next, using the relationship

$$P = f \oint H dB, \tag{2.17}$$

if the total power loss is divided by the frequency,

$$\frac{P_{\text{tot}}}{f} = k_{\text{hys}}(B) + k_{\text{eddy}}(B)f + k_{\text{exc}}(B)\sqrt{f}, \tag{2.18}$$

one finds that the same model can be used to find the effective field strength H. In other words, the part of H that contributes to magnetization rather than heat generation,

$$H_{\text{eff}}(B,f) = a(B) + b(B)f + c(B)\sqrt{f}. \tag{2.19}$$

2.6 Stress on underwater vessels

When the vessel is submerged, the water pressure deforms the hull. To compact this, beams are placed axially and tangentially inside the hull. The deformation is still present to a smaller degree, and the effect is most prevalent in between beams as shown in Fig. 2.4a.

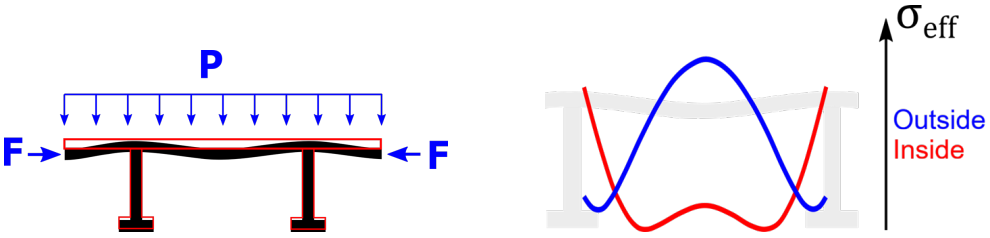

(a) Elastic hull deformations caused by water pressure.

(b) Stress diagram of hull cross section.

Figure 2.4: Hull subject to water pressure.

The stress diagram in Fig. 2.4b illustrates how the stress differs inside and outside the hull. The inward bending of the hull causes the inside to stretch and the outside to compress, which explains the characteristics of the diagram. Fig. 2.5 shows a simulation of a 4m submarine hull at 3.30 MPa, equivalent to a depth of about 330m.

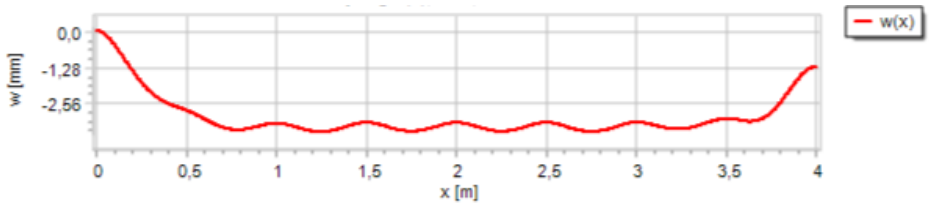

(a) Hull displacement at 3.30MPa water pressure.

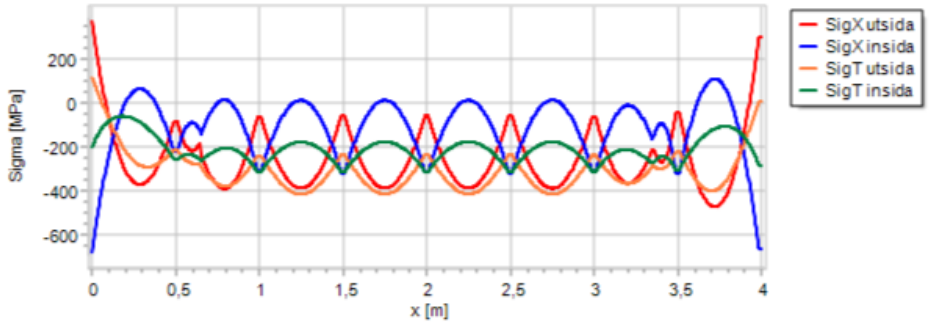

(b) Hull stresses at 3.30MPa water pressure. Red and blue represent the axial stresses on the outside and inside of the hull, respectively. Yellow and green represent the tangential stresses on the outside and inside of the hull, respectively.

Figure 2.5: Simulation of hull displacement and internal stresses at 3.30MPa water pressure.

As can be seen in this simulation, the stresses on the inside and outside of the hull are much greater than the water pressure, reaching a compressive stress

of about 400 MPa between the beams.

Chapter 3

Experimental setup

This chapter describes the experimental setup constructed to measure the magnetization of a steel sample under compressive stress. It begins with the sample itself, including its geometry, the simulated stress distribution under load, and the design of the copper solenoids, followed by the circuit used to generate the applied field and measure the induced voltage. The signal generation and data collection system is then described, along with the choice of output signal and sample rate. The chapter concludes with the data processing used to convert the measured voltages into hysteresis loops, the noise correction strategy, and an assessment of how eddy currents affect the results.

3.1 Samples

The sample used for the experiment was made of steel and was shaped as a thin transformer core, as can be seen in Fig. 3.1. The thin hole allows for a solenoid to be wrapped around each of the two segments, while keeping the stress distribution fairly homogeneous. This shape, compared to a rod or cuboid, also has the advantage of producing significantly higher magnetic flux. The relevant sample properties are presented in Table 3.1. As steel is composed primarily of iron, it is expected that the magnetostriction constant λ_s will be positive in the range of applied field strengths to which it will later be exposed. As such, the expected preferred domain direction will be the plane perpendicular to the direction of applied stress.

Property	Symbol	Value
Number of loops (solenoid 1)	N_1	90
Number of loops (solenoid 2)	N_2	90
Area (side segment)	A	4.43 cm^2
Mean magnetic path length	ℓ_m	20.1 cm

Table 3.1: Properties of the sample.

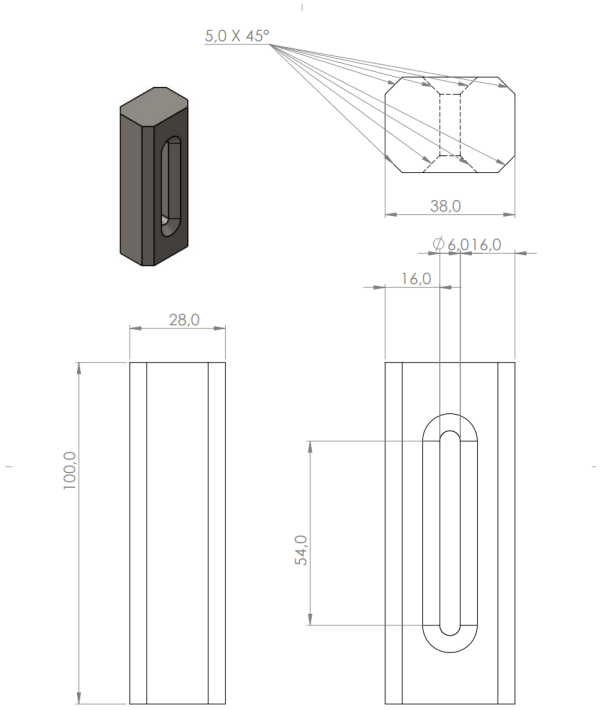

Figure 3.1: Sample blueprint, measurements in mm.

3.1.1 Stress distribution

Fig.3.2 shows a Finite Element Method (FEM) simulation of the sample under the maximum load used in the experiments, 250 kN. This was done in order to evaluate stress distribution inside the sample, specifically in the side segments where the magnetization is measured. The simulation shows a fairly even distribution of stress at approximately (300 ± 50)MPa, which is comparable to the values found in the 330m depth simulation.

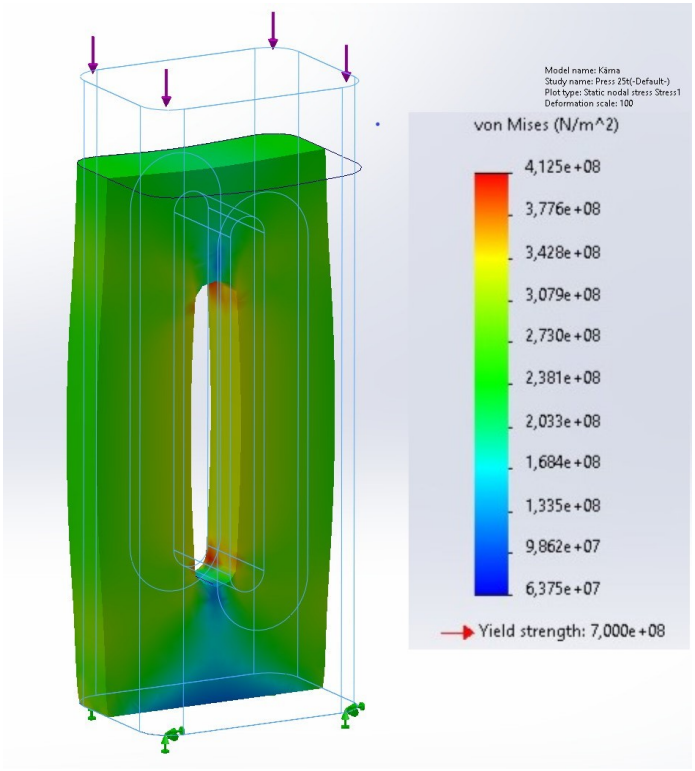

Figure 3.2: FEM simulation of the steel sample under 250 kN load.

3.1.2 Copper solenoids

When considering the thickness of copper wire and the number of loops for the solenoids, the factors that had to be considered were field strength, heat generation, and space available on the sample. Reaching magnetic saturation in the sample requires a strong enough magnetic field generated by solenoid 1. According to Eq. (2.4), the field strength scales linearly with both the number of loops and the current used.

$$H \propto IN \tag{3.1}$$

Furthermore, the heat generation in the copper wire, given by (2.7), is proportional to the current squared and the length of the wire, but also inversely proportional to the wire area.

$$P \propto I^2 \frac{l}{A} \tag{3.2}$$

Since the wire length is determined by how many loops fit on the solenoid, both the length and number of loops are, in this case, inversely proportional to the wire diameter. Hence, we can simplify the problem as follows.

$$H \propto I\frac{1}{r}, \qquad P \propto I^2\frac{1}{r^3}. \tag{3.3}$$

It is therefore more advantageous to increase the current rather than the number of loops. In the case of this setup, the power amplifier used had a maximum output of $15A$, so the goal was then to have enough loops in the solenoid, which required as thin a wire as possible, where heat was the limiting factor.

It was found that a 0.5mm diameter with 90 loops was enough to reach magnetic saturation with some margin. This thickness is not meant to be used at $15A$, however, by limiting measurement to $\sim$1-2 minutes, the heat was kept at an acceptable temperature (below 120°C). Furthermore, the sample was placed in a funnel connected to a fan to optimize cooling, and a temperature sensor was positioned on the copper wire such that the temperature could be continuously monitored during measurements.

For solenoid 2, heat generation will not be an issue since the circuit is not driven by current. In theory, an even thinner wire and more loops could have been used, as this would increase the measured voltage, thereby possibly contributing to better accuracy. For simplicity, the same wire was used, also with 90 loops.

Lastly, it should be noted that a layer of electrical tape was added to the side segments of the sample before the copper solenoid was wrapped around them. This was done for isolation as well as to accommodate a small expansion of the side segments under load. Because this layer was very thin, the loss in flux caused by the gap was considered insignificant.

3.2 Circuit

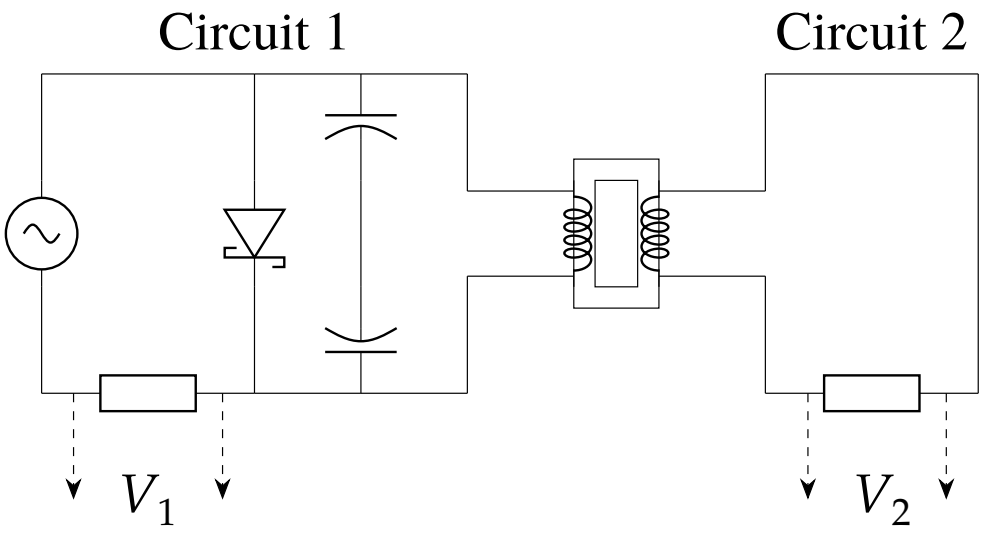

Figure 3.3: Circuit diagram of the experimental setup.

Fig. 3.3 illustrates the circuit used to generate the external field H and to measure the flux density B of the sample. In circuit 1, a AC signal is generated and sent through solenoid 1 to generate a high according to Eq. (2.4). The voltage in circuit 1 is continuously measured across the resistor R_1. To combat unwanted oscillations, a capacitor had to be connected in parallel to the solenoid. As no bipolar capacitors of enough strength were available, two polarized capacitors of equal strength ($2200\mu F$) connected in series, in opposite directions, were used instead. Lastly, for circuit 1, a bidirectional diode (Schottky diode) was connected in parallel to the solenoid to protect the system from a sudden discharge caused by self-inductance if the current in the solenoid were to drastically change. In circuit 2, the induced voltage was continuously measured to later calculate the magnetic flux using Eq. (2.3). It should be noted that the change in magnetization will only be measured in the direction of solenoid 2, which is parallel to the direction of applied stress.

3.3 Signal generation and data collection

The system was controlled using a compact real-time embedded industrial controller (cRIO), configured with analog input/output (IO) modules, programmed in LabVIEW. This device allows for calculations on IO signals,

data collection, and monitoring in real-time. In the setup of this experiment, the signal controlling the magnetic field in solenoid 1 was sent as an analog voltage signal from the cRIO to a power amplifier. Then the voltage in circuit 1 and circuit 2, and the weight signal from the hydraulic press scale were connected to the analog input module of the cRIO, where the data was collected.

3.3.1 Sample rate

The first version of the code was programmed in LabVIEW scan mode, a simpler mode in which all programming is done on the RT target and communication to the Field Programmable Gate Array (FPGA) is handled automatically. However, this mode is limited to a few hundred Hertz in sampling rate, which limits the speed with which the sine values of the output signal can be updated as well as the number of data points that can be collected. This mode was limited to about 200Hz, corresponding to 200 updates per period for a 1Hz sine wave output. In other applications, this would be a good approximation of a sine wave. However, since the field strength is proportional to the derivative of the signal, and every update of the output signal is close to a step function, this is enough to negatively impact the results. The sampling rate of the data collection was also too slow to accurately measure the voltage, creating unpredictable drifts in the voltage time integral.

In the second version of the code, the signal generation and data collection were programmed directly on the FPGA from which high-speed data streaming was used to transfer the results and write them to a file on the PC. This allowed for a much higher sampling rate. After some experimentation, an output update rate of 2kHz and a data sampling rate of 10kHz was chosen as a good compromise of accuracy and performance, fixing the issues mentioned above.

3.4 Output signal

The output signal used was a triangle wave for a few reasons. Mainly, it was easy to implement in LabVIEW, and compared to, for example, a sine wave, it has a constant derivative apart from the change in sign. A constant derivative is desirable since it makes eddy currents more predictable. In the code, the triangle wave was implemented as a Lookup Table (LUT) of one period in the range -1 to 1. For each output update the LUT was called using the relevant loop index. The value was then scaled by multiplication with the desired

amplitude. In the demagnetization protocol, the same signal was used, but the amplitude was slowly decreased linearly.

3.5 Data processing

3.5.1 Field calculations

The collected voltage data were analyzed using Python code that implements Eqs. (2.4) and (2.3). The voltage data from solenoids 1 and 2 are extracted from the data file as two NumPy arrays, ”V1” and ”V2” respectively. A Savitzky–Golay filter and a constant Direct Current (DC)-offset are applied to smooth the signal and compensate for noise, as discussed in more detail below. To calculate the magnetic flux at every data point, and subsequently the B field, the SciPY cumulative_trapezoid() function computes the cumulative integral of the voltage measured across solenoid 2 using the composite trapezoidal rule. The H field is obtained directly from the voltage across solenoid 1, and the magnetization M is then derived from B and H. After the field calculations, an integral offset correction is applied to the magnetization. Over time, we expect the M field to oscillate around zero, however, the initial curve offsets the cumulative integral, which has to be corrected for. This is done by shifting M such that its minimum and maximum values lie at an equal absolute value.

When plotting the calculated field points against each other the result is a H-M hysteresis diagram such as the one shown in Fig. 3.4.

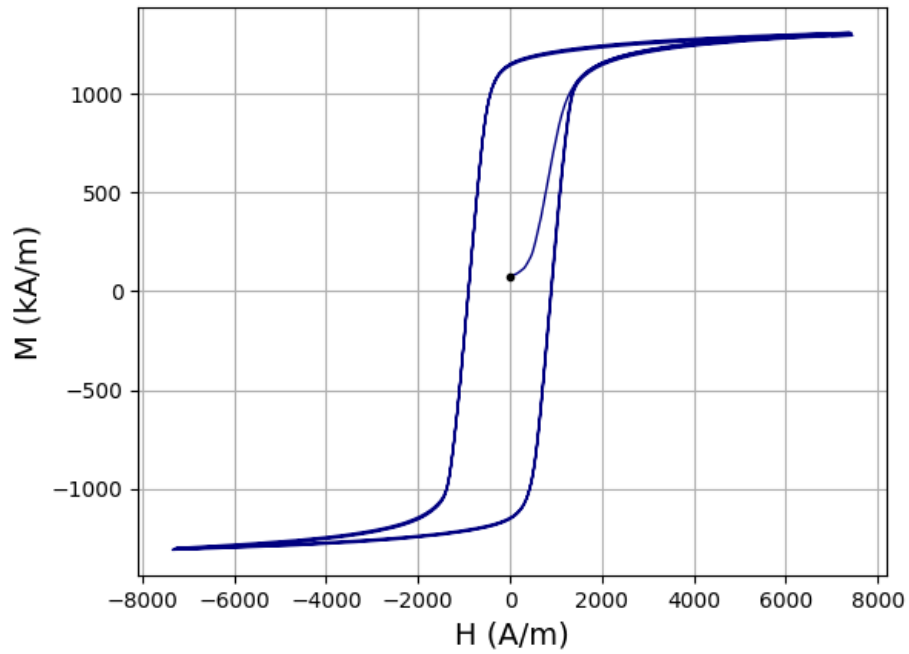

Figure 3.4: H-M diagram plotted in Python using measured voltage data.

3.5.2 Noise correction

The noise measurements, presented in Fig. 3.5, show oscillations at multiple frequencies centered around a positive DC-offset. The noise integral plot shows that using a Savitzky–Golay filter in combination with correcting the DC-offset using the mean value of the noise over time is an effective strategy to reduce the effect of noise in the field calculations.

The Savitzky–Golay filter smooths a signal by fitting a low-degree polynomial to successive windows of data points using linear least squares, replacing each point with the value of the fitted polynomial at its center [9]. This is done in order to suppress high-frequency noise.

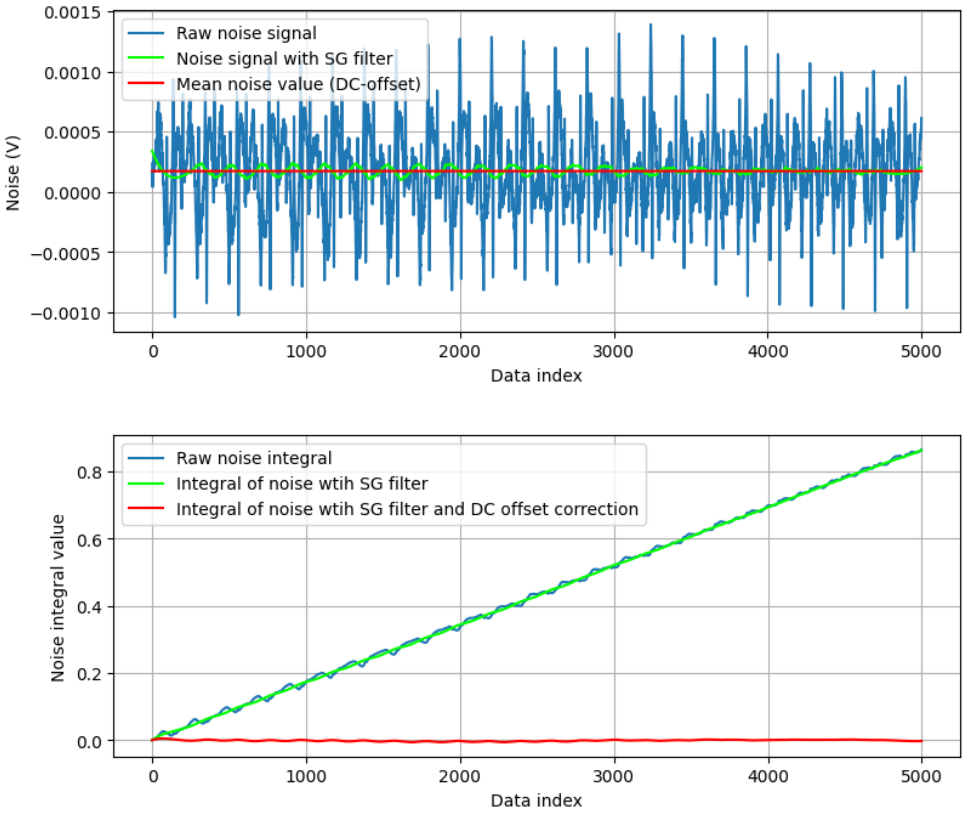

Figure 3.5: Noise signal and noise integral over a 0.5 second interval.

3.6 Effect of eddy currents

In theory, the magnetization of the sample at a given applied field strength should be independent of the rate of change in the applied field. In other words, the resulting H-M diagram should be the same regardless of which frequency is used in solenoid 1. However, this is where the effect of eddy current becomes problematic, as the magnetic field generated by eddy currents will also contribute to the measurement in solenoid 2. To further study this effect, several measurements were taken at varying low frequencies, these are presented in Fig. 3.6. The effect remains obvious even below 1 Hz. In an attempt to exclude the effect of eddy currents, the data from these measurements were extrapolated to zero frequency $f \rightarrow 0$. This was done by placing all measurements on a common grid consisting of 400 data points,

from which each data point had its frequency coefficients calculated. The model used was the aforementioned Bertotti model

$$H(B,f) = a(B) + b(B)f + c(B)\sqrt{f} \tag{3.4}$$

where a, b, c are the coefficients.

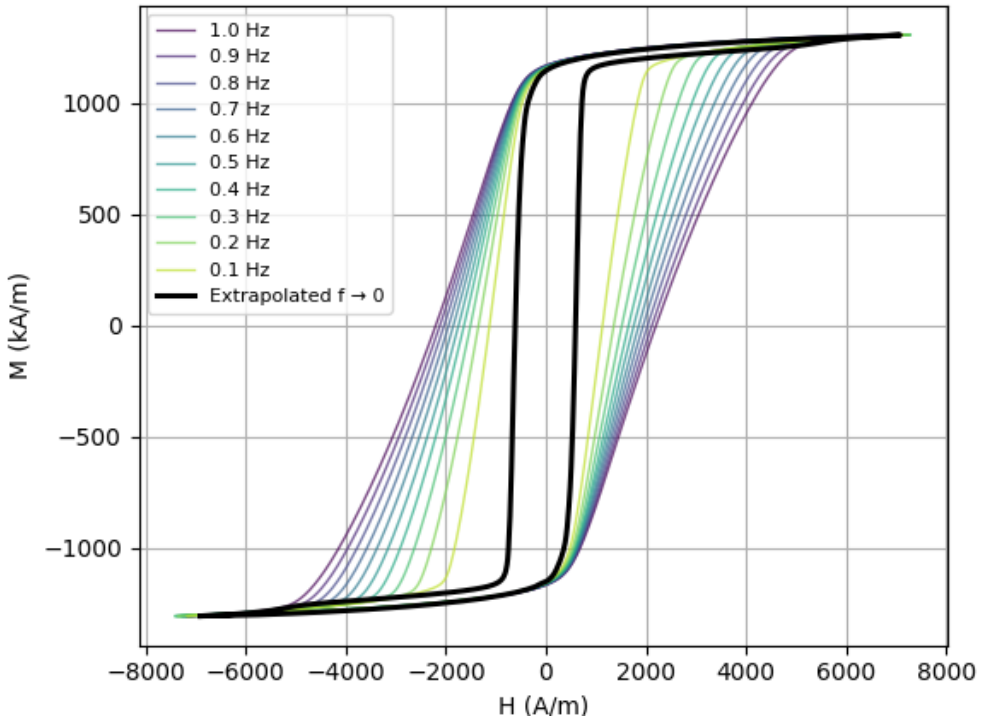

Figure 3.6: H-M loops measured at various frequencies with extrapolated loop $f \to 0$ in black.

To validate this model, predictions were made using the same coefficients at measurable frequencies, which were then compared to real measurements in Fig. 3.7a and 3.7b. The model shows promising accuracy, especially for predicting coercivity and remanence. However, there is a clear discrepancy between the prediction and measurements as the magnetization approaches saturation. Because of this, the implementation was not considered precise enough to artificially remove the contribution of eddy currents for the results using this model. Nevertheless, it does give a good perspective on how impactful eddy currents are in later results.

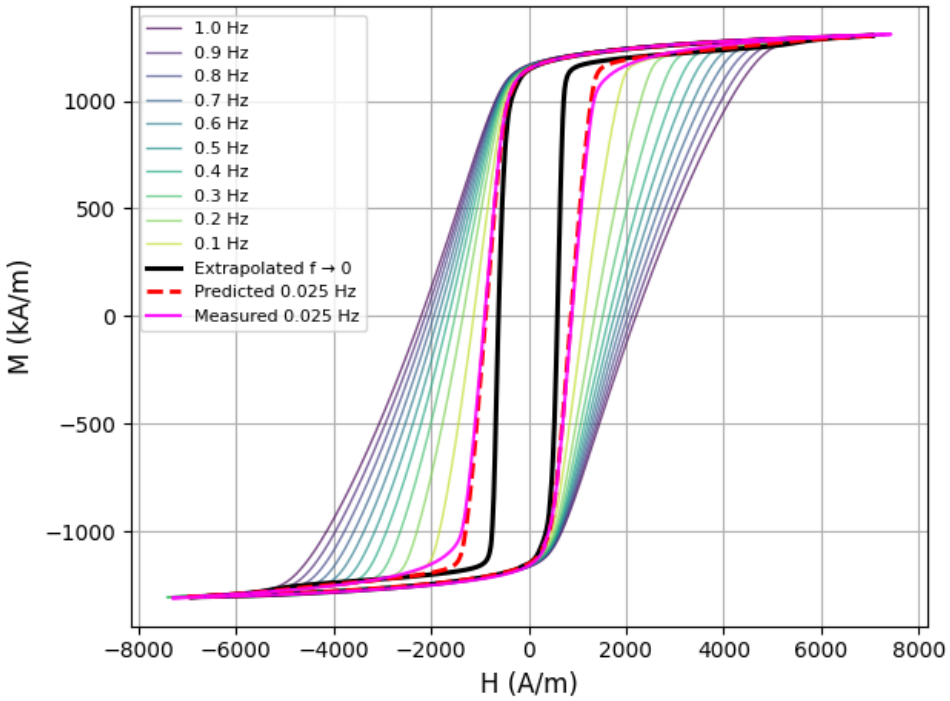

(a) H-M loop measured at various frequencies with extrapolated loop $f \to 0$ in black and predicted loop for $f = 0.25$Hz.

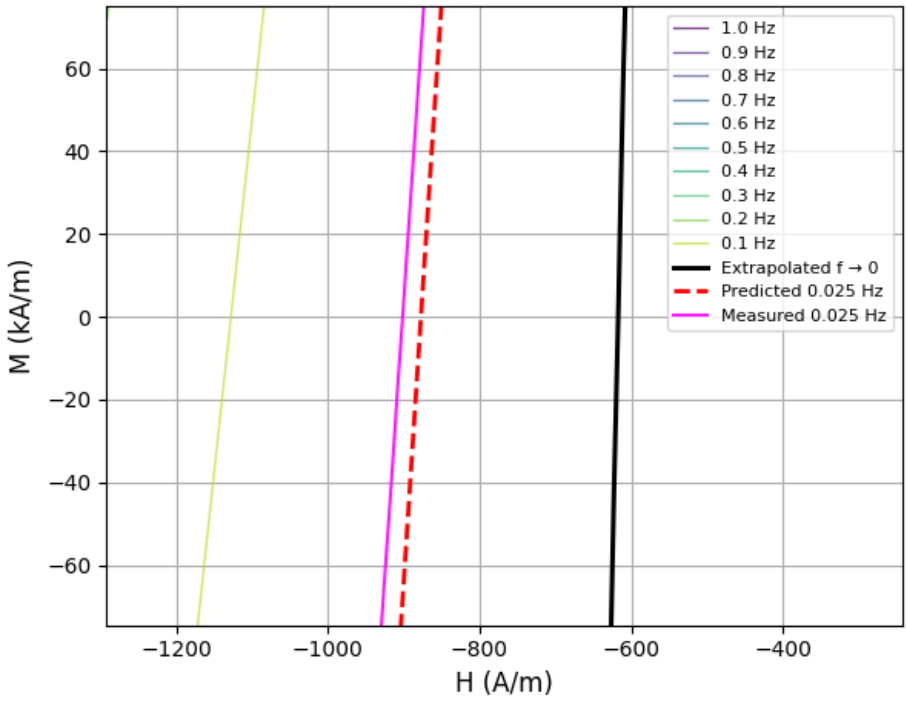

(b) Fig. 3.7a zoomed in near negative H_c.

Figure 3.7: Comparison between predicted H-M loop using Bertotti model and measured H-M loop for $f = 0.25$Hz.

Chapter 4

Experiment 1

4.1 Objective

The objective of the first experiment was to identify and compare the complete hysteresis loops of the sample under different compressive stress magnitudes. This was done to determine how magnetic properties, such as coercivity and remanent magnetization, vary with compressive stress.

4.2 Experiment procedure

Every measurement began by choosing a target load for that measurement. The sample was placed in the hydraulic press, and the load was manually increased until the target load was reached. This load was then held constant (within a 1% error margin) during the subsequent measurements. For each target load, the demagnetization protocol used a frequency of 1Hz and an initial amplitude of 15A, with a linear decay rate of 0.05A/s. Two measurements were taken at each target load, one with a signal of 15A, 0.025Hz, and one with 15A, 0.1Hz.

First, the demagnetization protocol was initiated. Once demagnetization was completed, the first noise measurement was taken. Then the 0.025Hz measurement was started and kept running for at least 120s, enough to complete 3 hysteresis loops. After that, the sample was demagnetized again before the 0.1Hz signal was recorded. This measurement was kept running for a minimum of 50s, completing at least 5 hysteresis loops. Lastly, another noise measurement was taken.

The procedure was then repeated for different loads, starting at 0 kN and increasing in increments of 50 kN up to 250 kN.

4.3 Results and analysis

All hysteresis loops using the 0.025Hz measurement are shown in figure 4.1. It is clear that all loops follow a trend, a higher applied load correlates with a wider hysteresis loop and an overall slower approach to magnetic saturation.

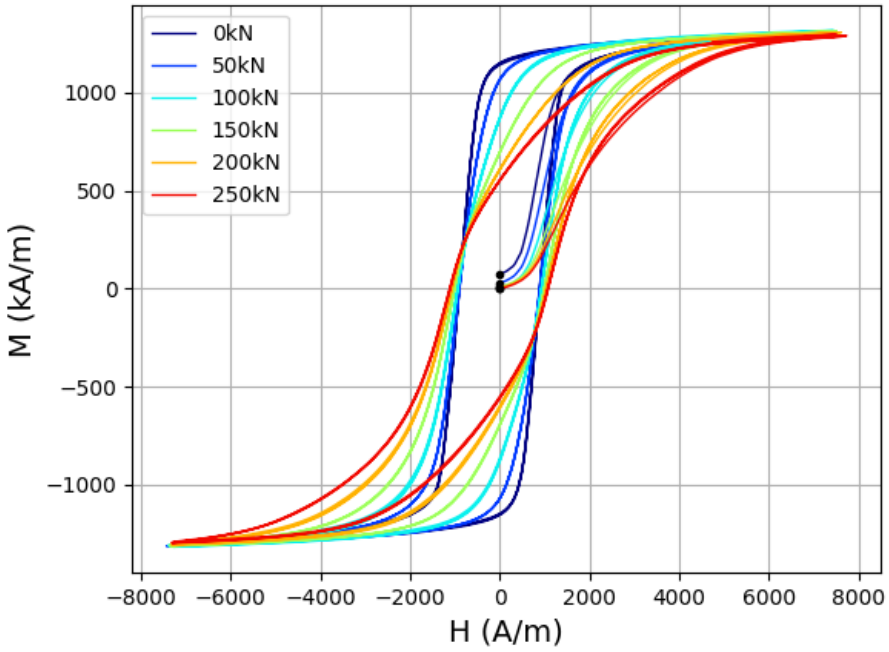

Figure 4.1: Average magnetization measured in the direction of stress against applied field strength, measured at six different loads using 15A, 0.025Hz, DC-offset corrected and applied Savitzky–Golay filter with window size of 501.

From the results in Fig. 4.1, the magnetic properties can be further analyzed by looking at the magnetic coercivity $H_c = |H(M = 0)|$ and magnetic remanence $M_r = |(M(H = 0)|$. These values are plotted against the compressive stress in Fig. 4.2. It becomes apparent that increased stress leads to higher magnetic coercivity and lower magnetic remanence. Although the behavior of the relationships is not entirely obvious from this data, it seems the change in coercivity is most drastic in the 100-200kN range, and for the remanence in the 50-150kN range.

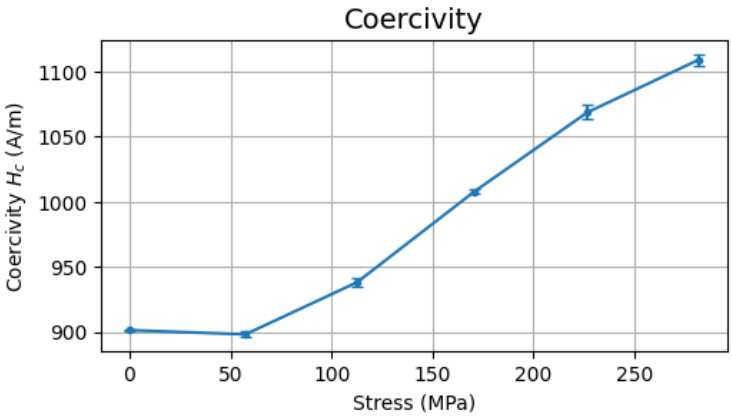

(a) Mean magnetic coercivity against compressive stress.

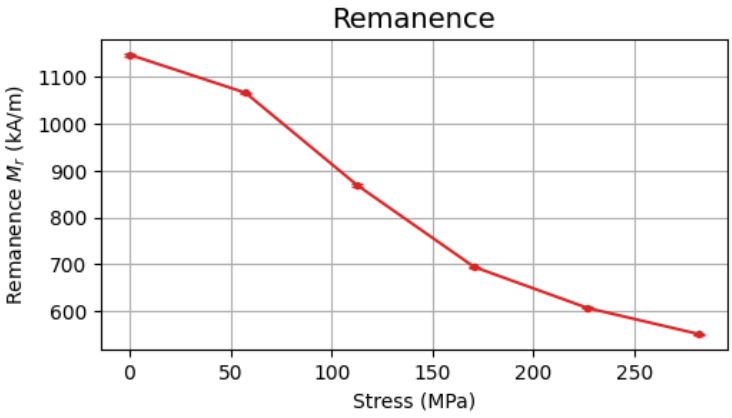

(b) Mean magnetic remanence against compressive stress.

Figure 4.2: Mean magnetic coercivity and remanence of the sample measured in the direction of stress against compressive stress, calculated from three loops, measured using 15A, 0.025Hz. Error bars show standard deviation across the three measurements.

This behavior is consistent with the magnetoelastic energy theory previously discussed for a material with a magnetostriction constant $\lambda_s > 0$. The compressive stress makes domain alignment unfavorable in the direction of the stress, driving the domains toward the perpendicular plane, in which magnetization is not measured. The sample requires a stronger field to become magnetized, and as the external field is removed, less magnetization remains.

Chapter 5

Experiment 2

5.1 Objective

The objective of the second experiment was to determine the change in absolute magnetization in a constant applied field as a function of compressive stress. This is in order to better understand the magneto-mechanical effect when stress is the only variable.

5.2 Experiment procedure

Before each stress measurement, a noise measurement was taken. Then, a constant DC signal was applied, and the voltage measurements were initiated. The load was then gradually increased from 0 to 250 kN. Since the hydraulic press required manual pumping, the stress increased rapidly during pumping but remained constant between pumps. Once 250 kN had been reached, the hydraulic press valve was carefully opened to release the stress smoothly. Once the pressure returned to zero, the measurement was complete. This procedure was first performed with no applied field. After that, the process was repeated using signals of 0.1A, 1A, and 10A. The corresponding field strengths of these signals, calculated using (2.4), are found in table 5.1. This experiment was first performed with the sample fully magnetized, meaning it had been exposed to a field strong enough that the remanent magnetization reached its maximum possible value (with no applied stress) and the domains were already aligned with the direction of stress. After that, the experiment was repeated with the sample demagnetized, so that the domains were randomly oriented.

Current I	Field strength H
0.1A	$\sim$ 44.8A/m^2
1A	$\sim$ 448A/m^2
10A	$\sim$ 4480A/m^2

Table 5.1: Current of DC signals used and corresponding field strengths in the solenoid.

5.3 Results and analysis

Fig. 5.1 shows the change in magnetization when compressive stress is applied to a fully magnetized sample under various constant field strengths. A clear decrease in magnetization is observed for all field strengths except the strongest, generated using 10A.

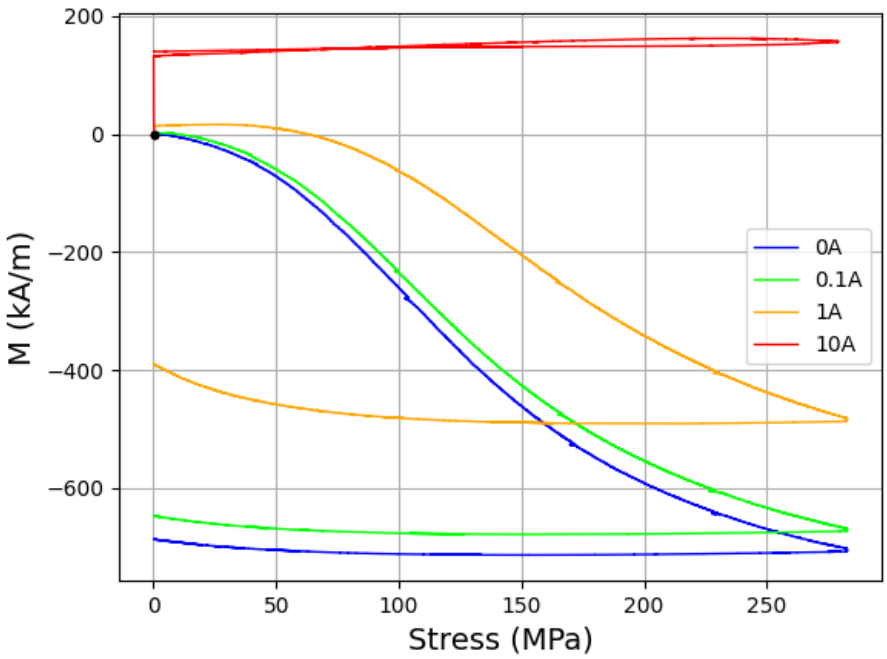

Figure 5.1: Change in magnetization measured in the direction of stress against applied stress in a fully magnetized sample subject to various constant applied field strengths.

The clear decrease in magnetization observed is further evidence of the findings from experiment 1. Since the sample is already magnetized

along the stress axis, the compressive stress destabilizes the existing domain configuration, reducing the net magnetization. It is worth noting that the curve with no applied field, apart from the geomagnetic field, exhibits a similar behavior to the remanence-stress relationship found in Fig 4.2.

At 10A, the sample is close to magnetic saturation, meaning the applied field is strong enough to largely overpower the magnetoelastic energy introduced by compression. The stress-induced drive toward perpendicular domain alignment is therefore insufficient to significantly disrupt the field-enforced configuration, and the magnetization remains approximately constant.

Fig. 5.2 shows the corresponding measurements for a demagnetized sample under the same range of field strengths. The results differ significantly.

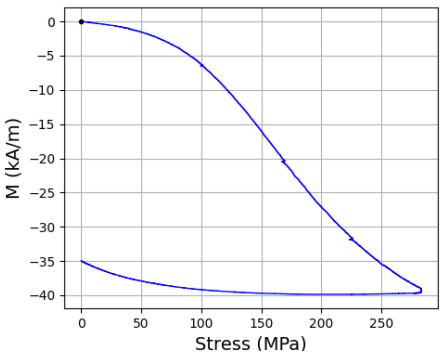

(a) Magnetization against stress subject only to the geomagnetic field.

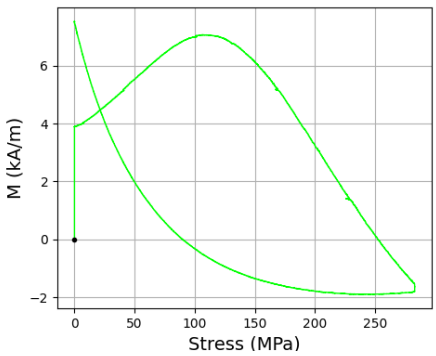

(b) Magnetization against stress in applied field generated using 0.1A DC.

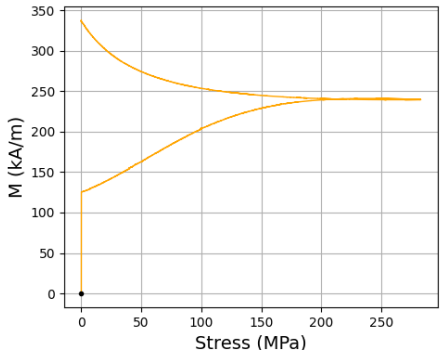

(c) Magnetization against stress in applied field generated using 1A DC.

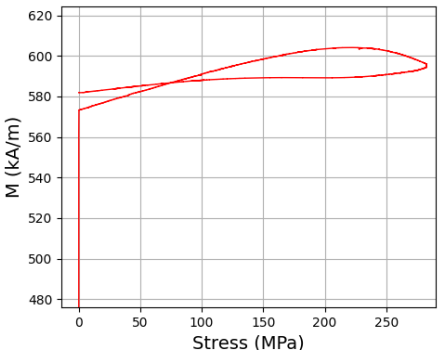

(d) Magnetization against stress in applied field generated using 10A DC.

Figure 5.2: Change in magnetization measured in the direction of stress against applied stress in a demagnetized sample subject to various constant applied field strengths.

In Fig. 5.2a, where the sample was subject only to the geomagnetic field, magnetization decreases with applied stress. This observation is mostly explained by the Villari effect counteracting the effect of the geomagnetic field. After the sample was demagnetized, it was still subject to the Earth's magnetic field, making it slightly favorable for domains to align in the same direction. In this case, the geomagnetic field is mostly aligned with the direction of stress, which is the same direction the sample is measured in. When stress is applied, the Villari effect makes the perpendicular plane more favorable, decreasing magnetization in the direction of measurement.

Under a 0.1A field (Fig. 5.2b), the change in magnetization it so small that the behavior might not be very meaningful. The most likely reason is

that the applied field is in a similar order of magnitude to the geomagnetic field, but facing the opposite direction. Therefore, no meaningful change it magnetization can be found in the direction of measurement.

Under a 1A field (Fig. 5.2c), magnetization increases both as stress is applied and upon its release, which is counterintuitive given that compression is expected to drive domains away from the measurement axis. A possible explanation is that stress cycling helps domain walls overcome pinning barriers, allowing more domains to settle into alignment with the field than before the stress was applied. However, this interpretation is speculative.

At 10A (Fig. 5.2d), the field is sufficiently strong that the sample behaves similarly to the fully magnetized case.

Chapter 6

Discussion

The setup used shows promising capability and accuracy in identifying even very small changes in the samples' magnetization. Although data redundancy is very limited in this study, the standard deviation in experiment 1 indicates high precision and effective noise handling.

The results indicate a clear correlation between magnetization and compressive stress in steel, affecting magnetic properties such as coercivity and remanence, and directly changing the direction of domains. For a material with $\lambda_s > 0$ under compression parallel to an applied field, the energetically preferred domain orientation is perpendicular to the field. Domains already aligned with the field are therefore destabilized, increasing the energy barrier for domain wall motion, raising coercivity, and reducing remanence. This mechanism is broadly reported for soft magnetic materials under compressive stress [10].

Although this experimental setup cannot measure magnetization perpendicular to the stress direction, the Villari effect suggests that a demagnetized sample would exhibit an increase in magnetization in that direction. Similarly, in Eq. (2.1), switching the sign, or direction, of the stress σ, would make the direction of stress the preferred direction of domain orientation. It is therefore reasonable to assume that a demagnetized sample subject to tensile stress would see an increase in magnetization in the direction of stress, with similar behavior of 5.1, but increasing instead of decreasing. This is also consistent with similar studies [11] and would be measurable with the circuit used in this study if a way could be found to apply tensile stress.

In the context of underwater naval systems, these results highlight two important considerations. Firstly, if a demagnetized vessel is submerged, one should expect a substation reintroduction of magnetization perpendicular to

the direction of compressive stress. Secondly, if countermeasures are to be implemented to reduce the magnetic signature, they must account for the stress dependence of the material's magnetic properties, as observed in experiment 1.

6.1 Limitations

It is important to note that the values produced in these experiments is heavily dependent on the ferromagnetic material used, as the hysteresis behavior may differ greatly. This study should be interpreted as a demonstration of how magnetization can be measured under stress and as an indication of the behavior to expect.

Furthermore, the influence of eddy currents in experiment 1 is significant to a degree that the results are strictly qualitative, even for the specific material at hand.

6.2 Conclusions

An experimental setup that allows one to measure magnetic properties in magnetic cores subject to compressive stress was constructed. The setup was capable of real time data collection during various external field and stress cycles. It showed promising capability and accuracy, although the influence of eddy currents persists as an error source for measurements in alternating external fields, even at very low frequencies.

Measurements confirmed a clear stress dependence of coercivity and remanence, consistent with magnetoelastic theory for a material with $\lambda_s > 0$. Compressive stress parallel to the applied field drives domains toward the perpendicular plane, raising coercivity and reducing remanence in a manner that scales continuously with applied stress across the tested range.

The demagnetized sample measurements conducted in experiment 2 indicate a stress-induced remagnetization perpendicular to the direction of stress. However, more experimentation is needed in order to draw any conclusions about its behavior.

6.3 Future work

6.3.1 Possible setup improvements

The main area for improvement is reducing the setup's heat generation, as it currently limits how long measurements can be conducted under a strong field. Allowing longer measurement would make it possible to collect more hysteresis loops in experiment 1, which could be used to increase accuracy. It would also allow measurement at a lower frequency, thereby reducing the effects of eddy currents. Reducing heat can be done in multiple ways. As previously discussed, one approach would be to increase the copper wire's diameter. This would also mean fewer loops in the solenoids would fit on the sample, lowering the maximum field strength, however, increasing the current to maintain the same field strength would, in this scenario, still lead to less heat. One could also improve cooling with a stronger fan and an improved funnel, concentrating the cooling around the field-generating solenoid.

Another improvement, which was implemented for experiment 2 of this study but not before experiment 1, was the use of a signal amplifier for the voltage readings across circuits 1 and 2. This allows detection of smaller variations in the fields that would otherwise be heavily influenced by noise. This was crucial for experiment 1, as the voltage generated in circuit 2, due to stress-induced magnetization, was much smaller than the voltage induced by the time-varying external field. If experiment 1 were to be repeated using lower frequencies, using a signal amplifier could be more essential, as the smaller flux derivative would also induce less voltage in circuit 2.

When it comes to the signal used to generate the external field, there are signals that could be more advantageous than a simple triangle wave for reducing eddy currents, or at least make removing the effect in models more reliable. Looking back at Fig. 3.6, the eddy current effect is most pronounced as the sample approaches magnetic saturation. This is likely because the decay time of the eddy currents is long enough that they build up over time when the field derivative is at its largest point. To combat this, one could limit the signal change to small increments, keeping it constant in between intervals, giving the eddy currents time to decay.

6.3.2 Further experiments

Using the experimental setup of this experiment, it would be interesting to further study the Villari effect by repeating experiment 2 with tensile stress

instead of compressive stress. That way, one could measure the increase in magnetization for a demagnetized sample in the direction where the change, in theory, should be most prevalent. Originally, this was planned to be a part of this study, however, modifying the hydraulic press turned out to be outside the time scope of the project.

One could also conduct other variants of experiment 1, for example, apply multiple stress cycles within a single measurement, each repeating the same stress cycle multiple times, or increase the maximum load with each cycle. This could then give further insight into how repeated stress impacts magnetization. This could also be a more realistic representation of how a naval vessel might be used after its demagnetization.

It would also be interesting to investigate how the stress dependence of magnetization behaves at higher stress levels than those achievable with the sample and hydraulic press in this setup.

6.4 Use of AI tools

In this thesis, generative AI was used to correct grammar and improve clarity by restructuring certain sentences. It was also used as an aid in implementing the Berotti model in Python, specifically where measured data had to be placed on a common grid.

References

[1] B. D. Cullity and C. D. Graham, *Introduction to Magnetic Materials*, 2nd ed. Wiley-IEEE Press, 2009. [Online]. Available: https://www.wiley.com/en-us/Introduction+to+Magnetic+Materials%2C+2nd+Edition-p-9780471477419

[2] D. J. Griffiths, *Introduction to Electrodynamics*, 4th ed. Pearson, 2013. ISBN 978-0-321-85656-2

[3] Gorchy. NdFeB-Domains.jpg. Wikimedia Commons. Licensed under CC BY-SA 3.0 Unported. [Online]. Available: https://commons.wikimedia.org/wiki/File:NdFeB-Domains.jpg

[4] W. A. Thurber, "Magnetizing and demagnetizing with alternating currents," *School Science and Mathematics*, vol. 43, no. 9, pp. 824–827, 1943.

[5] D. C. Jiles, "Theory of the magnetomechanical effect," *Journal of Physics D: Applied Physics*, vol. 28, no. 8, p. 1537. doi: 10.1088/0022-3727/28/8/001. [Online]. Available: https://doi.org/10.1088/0022-3727/28/8/001

[6] T. M. Baynes, "Analysis of the demagnetisation process and possible alternative magnetic treatments for naval vessels," PhD thesis, UNSW, Australia, 2002. [Online]. Available: http://hdl.handle.net/1959.4/20479

[7] I. D. Vagner, B. I. Lembrikov, and P. Wyder, *Electrodynamics of Magnetoactive Media*, ser. Springer Series in Solid-State Sciences. Springer, vol. 135. ISBN 978-3-642-07825-5 978-3-662-06941-7. [Online]. Available: http://link.springer.com/10.1007/978-3-662-06941-7

[8] G. Bertotti, "General properties of power losses in soft ferromagnetic materials," *IEEE Transactions on Magnetics*, vol. 24, no. 1, pp.

621–630. doi: 10.1109/20.43994. [Online]. Available: https://ieeexplore.ieee.org/document/43994/

[9] A. Savitzky and M. J. E. Golay, "Smoothing and differentiation of data by simplified least squares procedures," *Analytical Chemistry*, vol. 36, no. 8, pp. 1627–1639, 1964. doi: 10.1021/ac60214a047

[10] S. Toyting, C. W. Harrison, A. Lambourne, and H. J. Stone, "Magnetic behaviour of FeCo-2V under applied stress and elevated temperature," *Materialia*, vol. 45, p. 102636, 2026. doi: 10.1016/j.mtla.2025.102636. [Online]. Available: https://doi.org/10.1016/j.mtla.2025.102636

[11] C. A. Ives, S. G. H. Staples, C. K. Vo, D. M. J. Cowell, S. Freear, and B. T. H. Varcoe, "Toward using the villari effect for non-destructive evaluation of steel structures," *Journal of Applied Physics*, vol. 134, no. 6, p. 065101. doi: 10.1063/5.0147736. [Online]. Available: https://doi.org/10.1063/5.0147736

TRITA – SCI-GRU 2026:302
Stockholm, Sweden 2026

www.kth.se

€€€€ For DIVA €€€€

{
”Author1”: { ”Last name”: ”Käll”,
”First name”: ”Niklas”,
”Local User Id”: ”nkall”,
”E-mail”: ”nkall@kth.se”,
”organisation”: {”L1”: ”School of Engineering Sciences”,
}
},
”Cycle”: ”2”,
”Course code”: ”SK202X”,
”Credits”: ”30.0”,
”Degree1”: {”Educational program”: ”Master’s Programme, Engineering Physics, 120 credits”
,”programcode”: ”TTFYM”
,”Degree”: ”Degree of Master of Science in Engineering”
,”subjectArea”: ”Applied Physics”
},
”Title”: {
”Main title”: ”Towards understanding magnetization in underwater naval systems”,
”Subtitle”: ”Measuring magnetic properties in steel subject to water pressure induced stress”,
”Language”: ”eng” },
”Alternative title”: {
”Main title”: ”Mot en ökad förståelse av magnetisering i undervattensfarkoster”,
”Subtitle”: ”Mätning av magnetiska egenskaper hos stål utsatt för vattentrycksinducerad spänning”,
”Language”: “swe”
},
”Supervisor1”: { ”Last name”: ”Djurberg”,
”First name”: ”Viktor”,
”E-mail”: ”viktor.djurberg@foi.se”,
”Other organisation”: ”Swedish Defence Research Agency (FOI)”
},
”Supervisor2”: { ”Last name”: ”Hagström”,
”First name”: ”Nanna Zhou”,
”E-mail”: ”nanna.zhou.hagstrom@foi.se”,
”Other organisation”: ”Swedish Defence Research Agency (FOI)”
},
”Supervisor3”: { ”Last name”: ”Åkerstedt”,
”First name”: ”Henrik”,
”E-mail”: ”henrik.akerstedt@foi.se”,
”Other organisation”: ”Swedish Defence Research Agency (FOI)”
},
”Examiner1”: { ”Last name”: ”Andersson”,
”First name”: ”Magnus”,
”Local User Id”: ”magnusan”,
”E-mail”: ”magnusan@kth.se”,
”organisation”: {”L1”: ”School of Engineering Sciences”,
”L2”: ”Applied Physics” }
},
”Cooperation”: { ”Partner_name”: ”Swedish Defence Research Agency (FOI)”},
”National Subject Categories”: ”103, 10304”,
”Other information”: {”Year”: ”2026”, ”Number of pages”: ”x,38”},
”Copyrightleft”: ”copyright”,
”Series”: { ”Title of series”: ”TRITA – SCI-GRU” , ”No. in series”: ”2026:302” },
”Opponents”: { ”Name”: ””},
”Number of lang instances”: ”2”,
”Abstract[eng]”: €€€€

Stealth is a key attribute of underwater naval systems, many of which are built from ferromagnetic materials such as steel. These materials can retain a permanent magnetization, producing a detectable magnetic signature, so vessels are typically demagnetized before deployment. When submerged, however, water pressure imposes compressive stress on the hull, which can reintroduce magnetization via the Villari effect. This thesis investigates the relationship between compressive stress and the magnetic properties of ferromagnetic materials under high water pressure conditions.

An experimental setup was constructed to measure the magnetization of a steel core sample under controlled compressive stress, using a hydraulic press and a two-solenoid arrangement to generate an applied field and measure magnetic flux. Two experiments were performed. In the first, hysteresis loops were recorded under an alternating applied field at several constant stress levels. The loops widened with increasing stress, corresponding to increased magnetic coercivity and decreased remanence. In the second experiment, the change in magnetization was measured under a constant applied field while the stress was varied. A fully magnetized sample showed a clear decrease in magnetization with stress at all but the strongest applied field, whereas the demagnetized sample exhibited more complex behavior.

The observed stress dependence is consistent with magnetoelastic theory for a material with positive saturation magnetostriction, in which compressive stress drives domains away from the stress axis.

Eddy currents were found to influence the alternating-field measurements significantly, even below 1 Hz, limiting those results to a qualitative interpretation. The findings indicate that the stress dependence of magnetic properties should be accounted for when counteracting the magnetic signature of underwater naval systems.

"Abstract[swe]": €€€€

Smygförmåga är en central egenskap hos undervattensfarkoster, varav många är byggda av ferromagnetiska material såsom stål. Dessa material kan behålla en permanent magnetisering och därmed ge upphov till en detekterbar magnetisk signatur, varför farkoster vanligtvis avmagnetiseras innan användning. Vid nedsänkning utsätter dock vattentrycket skrovet för tryckspänning, vilket kan återintroducera magnetisering via Villari-effekten. Detta examensarbete undersöker sambandet mellan tryckspänning och de magnetiska egenskaperna hos ferromagnetiska material under förhållanden med högt vattentryck.

En experimentuppställning konstruerades för att mäta magnetiseringen hos ett stålprov i form av en kärna under kontrollerad tryckspänning, detta med hjälp av en hydraulisk press och en uppställning bestående av två solenoider för att generera ett pålagt fält och mäta det magnetiska flödet. Två experiment genomfördes. I det första undersöktes hystereskurvor under ett alternerande pålagt fält vid flera konstanta spänningsnivåer. Kurvorna vidgades med ökande spänning, vilket motsvarar ökad koercivitet och minskad remanens. I det andra mättes förändringen i magnetisering under ett konstant pålagt fält medan spänningen varierades. Ett fullt magnetiserat prov uppvisade en tydlig minskning av magnetiseringen med spänning vid alla fält utom det starkaste, medan det avmagnetiserade provet uppvisade ett mer komplicerat beteende.

Det observerade spänningsberoendet stämmer överens med magnetoelastisk teori för ett material med positiv magnetostriktionskonstant, där tryckspänning driver domänerna bort från spänningsaxeln. Virvelströmmar visade sig påverka mätningarna i alternerande fält avsevärt, även vid frekvenser lägre än 1 Hz, vilket begränsar dessa resultat till en kvalitativ tolkning. Resultaten indikerar att magnetiska egenskapers spänningsberoende bör beaktas vid utformningen av motmedel mot undervattensfarkosters magnetiska signatur.

€€€€,
"Keywords[eng]": €€€€
Magnetism, Ferromagnetism, Villari effect, Magnetoelastic coupling, Magnetic hysteresis, Coercivity, Remanence, Demagnetization, Underwater naval systems
€€€€,
€€€€,
"Keywords[swe]": €€€€
Magnetism, Ferromagnetism, Villari-effekten, Magnetoelastisk koppling, Magnetisk hysteres, Koercivitet, Remanens, Avmagnetisering, Undervattensfarkoster
€€€€,
}

acronyms.tex

```
%%% Local Variables:
%%% mode: latex
%%% TeX-master: t
%%% End:
\setabbreviationstyle[acronym]{long-short}

\newacronym{FOI}{FOI}{Swedish Defence Research Agency}
\newacronym{AC}{AC}{Alternating Current}
\newacronym{DC}{DC}{Direct Current}
\newacronym{MAD}{MAD}{Magnetic Anomaly Detector}
\newacronym{FPGA}{FPGA}{Field Programmable Gate Array}
\newacronym{cRIO}{cRIO}{compact real-time embedded industrial controller}
\newacronym{IO}{IO}{input/output}
\newacronym{FEM}{FEM}{Finite Element Method}
\newacronym{LUT}{LUT}{Lookup Table}
\newacronym{JAS}{JAS}{Jiles-Atherton-Sablik}
```

Empty list